Environmental Science & Technology

pubs.acs.org/est

Article

A Novel Lab-on-Chip Spectrophotometric pH Sensor for Autonomous *In Situ* Seawater Measurements to 6000 m Depth on Stationary and Moving Observing Platforms

Tianya Yin, Stathys Papadimitriou, Victoire M.C. Rérolle, Martin Arundell, Christopher L. Cardwell, John Walk, Martin R. Palmer, Sara E. Fowell, Allison Schaap, Matthew C. Mowlem, and Socratis Loucaides*

Cite This: *Environ. Sci. Technol.* 2021, 55, 14968−14978

Read Online

ACCESS | Metrics & More | Article Recommendations | Supporting Information

ABSTRACT: We report a new, autonomous Lab-on-Chip (LOC) microfluidic pH sensor with a 6000 m depth capability, ten times the depth capability of the state of the art autonomous spectrophotometric sensor. The pH is determined spectrophotometrically using purified *meta*-Cresol Purple indicator dye offering high precision (<0.001 pH unit measurement reproducibility), high frequency (every 8 min) measurements on the total proton scale from the surface to the deep ocean (to 600 bar). The sensor requires low power (3 W during continuous operation or ∼1300 J per measurement) and low reagent volume (∼3 μL per measurement) and generates small waste volume (∼2 mL per measurement) which can be retained during deployments. The performance of the LOC pH sensor was demonstrated on fixed and moving platforms over varying environmental salinity, temperature, and pressure conditions. Measurement accuracy was +0.003 ± 0.022 pH units (n = 47) by comparison with validation seawater sample measurements in coastal waters. The combined standard uncertainty of the sensor *in situ* pH_T measurements was estimated to be ≤0.009 pH units at pH 8.5, ≤ 0.010 pH units at pH 8.0, and ≤0.014 pH units at pH 7.5. Integrated on autonomous platforms, this novel sensor opens new frontiers for pH observations, especially within the largest and most understudied ecosystem on the planet, the deep ocean.

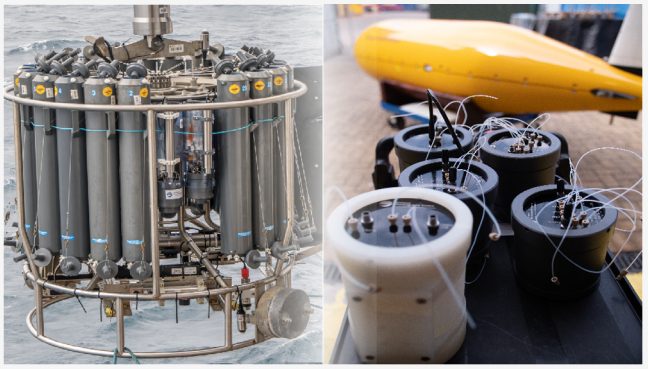

KEYWORDS: *pH sensors, spectrophotometric, deep ocean, autonomous platforms, mCP, lab-on-a-chip, ocean acidification*

Downloaded via 82.11.180.11 on May 28, 2026 at 14:19:54 (UTC).
See https://pubs.acs.org/sharingguidelines for options on how to legitimately share published articles.

1. INTRODUCTION

The oceans absorb about a quarter of anthropogenic CO_2 emissions[1] at a rate of 2−3 Pg C yr^{-1}.[2] As a result, surface ocean pH has decreased by an estimated 0.1 pH units since the onset of the industrial revolution[3] at an average rate of 0.002 pH units per year. Ocean acidification alters dissolved inorganic carbon (DIC) speciation, leading to lower saturation state (Ω), with respect to the $CaCO_3$ polymorphs (calcite, aragonite), of the shells and skeletons of many (calcifying) marine organisms. Ocean acidification, therefore, poses a threat to marine ecosystem functioning and the ocean-based economy,[4−8] with projections for surface water undersaturation (Ω < 1) in parts of the global ocean by the end of this century.[9] The response of calcifying organisms to varying levels of Ω[5,7,10,11] has rendered this parameter a key ocean acidification indicator for the assessment of ecosystem effects.[12,13] In order to characterize biologically meaningful spatial patterns and short-term variations in ocean acidification, the maximum uncertainty should be ±0.2 in the calculation of Ω (weather goal)[12,13] from measurements of two of the five directly measurable carbonate system parameters, DIC, total alkalinity (TA), the fugacity of CO_2 (fCO_2), CO_3^{2-}, and pH = $-\log[H^+]$,[14]. Current analytical uncertainties[15] indicate achievement of weather goal Ω uncertainty through paired measurements of pH and DIC, pH and TA, or DIC and fCO_2 by expert analysts using state-of-the-art laboratory techniques and instrumentation. The ambition of the ocean observing community, however, is that such high-quality measurements can be made autonomously on marine monitoring platforms allowing changes in marine carbonate chemistry to be monitored *in situ* at a high spatial and temporal scale from

Received: May 31, 2021
Published: October 13, 2021

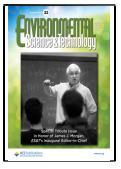

ACS Publications

© 2021 The Authors. Published by American Chemical Society

surface waters to the deep ocean. This capability will also allow for better and direct quantification of the oceanic carbon budget including CO_2 fluxes with the atmosphere. The main obstacle in making this vision reality has been the lack in autonomous sensor technology capable of long-term unassisted carbonate chemistry observations on small marine autonomous platforms, especially at high pressures.[16]

Recent advances in electrochemical pH sensor technology have provided the first unassisted, long-term measurements of ocean pH using profiling floats.[17] Sensors for ocean pH measurements using the Ion-Sensitive Field Effect Transistor (ISFET) potentiometric technology of the Honeywell DuraFET[18] have demonstrated Nernstian response and stability in seawater over several months of continuous deployment with <0.010 pH unit accuracy.[19,20] Commercially available sensors based on this technology (seaFET and seapHOx; Sea-Bird Scientific) have a maximum depth rating of 2000 m and quoted accuracy of 0.050 pH units (https://www.seabird.com/seafet-v2-ocean-ph-sensor). Electrochemical pH sensors (e.g., seaFET) can provide the high frequency (10 Hz maximum) measurements required for fast moving platforms but have limitations, including long conditioning times (5−10 days) and long-term electrode response drift.[17,19,21−23] Integrated on Biogeochemical Argo floats, seaFET sensors have been reporting pH data for more than a decade.[24] Periodic drift correction at 2000 m depth improves dramatically long-term pH measurement performance, and coupled with empirically estimated TA, the marine carbonate system speciation including Ω and fCO_2 can be approximated in near-real time.[24,25]

Since the 1980s, the standard analytical method for the measurement of pH in seawater is the spectrophotometric technique using sulfonephthaleine pH indicator dyes[26,27] with demonstrated precision of <0.001 pH units[26] and accuracy of <0.010 pH units.[28−30] Because it requires benchtop spectrophotometers with thermostated and, ideally, stirred glass cuvettes,[31] the application of this technique for autonomous devices presents more complexity than electrochemical techniques. Over the last two decades, Sunburst Sensors (www.sunburstsensors.com) has been developing spectrophotometric pH sensors (SAMI-pH) for autonomous moored deployments.[32,33] The SAMI-pH offers high-performance autonomous pH measurements on stationary platforms and has been widely adopted by the ocean carbon observing community, but, because of its size (55 × 15 cm) and limited pressure tolerance (<60 bar), its use is restricted to shallow moored applications.

Since its introduction in the 1990s, Lab-on-Chip (LOC) technology has attracted interest in its application to many fields because it allows miniaturization of analytical systems with its custom-designed microfluidic manifolds, integrated mini-valves, pumps, and other features.[34] Integration of fluidic components within microfluidic chips reduces footprint and manufacturing costs.[35] By allowing application of standard, high-performance analytical methods to small devices with low power and reagent requirements, LOC technology offers great potential for autonomous observations on fixed and moving monitoring platforms. LOC-based devices have been in development in our laboratory for the past decade for macro-nutrient[36,37] and dissolved iron and manganese measurements.[38,39] The hardware platform, currently at version 3.3, has been demonstrated both on stationary and autonomous moving platforms.[36−41] One of its greatest advantages is its high-pressure tolerance (at least to 600 bar) opening new frontiers into the largely unexplored and undersampled deep ocean.[42] The importance of deep ocean processes in climate regulation and carbon storage is now widely recognized[42,43] and a global effort to expand observations below 200 m is currently underway, coordinated by the Global Ocean Observing System (GOOS) through its Deep Ocean Observing Strategy (DOOS; https://deepoceanobserving.org/). Although temporal changes in deep ocean carbonate chemistry are slow (decades to centuries), spatial variability driven by geochemical and physical processes (hydrothermal activity, deep-water formation, etc.) is still not well documented. Furthermore, recent interest in deep ocean mining and storage of CO_2 has highlighted the urgent need for autonomous observing systems capable of sustained deep-water observations, both for environmental baselining and detection of anthropogenic perturbations. For monitoring subseabed CO_2 storage sites, for example, deviation in seawater pH from background variability is used as a proxy for CO_2 leakage into the overlying water[44] and, therefore, the availability of high precision pH sensors capable of autonomous measurements at depth is of paramount importance. In this paper, we describe the first ever autonomous spectrophotometric pH sensor, capable of high performance pH measurements, from the surface to the deep ocean (to 6000 m) integrated on stationary and underwater autonomous/robotic platforms.

2. MATERIALS AND METHODS

2.1. Measurement Principle. The LOC sensor determines pH on the total proton scale (pH_T) spectrophotometrically using purified *meta*-Cresol Purple (mCP) solution. The sensor measures pH_T ($pH_{T,m}$) at the temperature within the optical cell (t_m) (section 2.2) according to[45]

$$pH_{T,m} = -\log(K_2 e_2) + \log\left(\frac{R - e_1}{1 - R\frac{e_3}{e_2}}\right) \quad (1)$$

The *in situ* pH_T can then be derived from $pH_{T,m}$ and the *in situ* temperature (t) ($pH_{T,t}$) using the linear temperature factor[46] as follows

$$pH_{T,t} = pH_{T,m} - 0.01582(t - t_m) \quad (2)$$

In eqs 1 and 2 above, K_2 is the second stoichiometric (concentration-based) equilibrium dissociation constant of mCP, e_1, e_2, and e_3 are the ratios of the molar extinction coefficients of mCP, and R = A_{578}/A_{434} is the conventional ratio of absorbances (A_λ) at the absorbance maximum wavelengths (λ), 434 and 578 nm, of the protonated and deprotonated mCP species, respectively. The LOC sensor optics (Sensor Hardware) yield absorbance ratios (R_{meas}) corrected for sample pH perturbation in the presence of mCP (Calculation of Absorbance and Sample pH Correction for Indicator Perturbation), followed by adjustment to the conventional R via calibration with Tris-HCl buffers (Standardization of R_{meas}). For sensor pH determination (eq 1), $-log(K_2e_2)$, e_1, and e_3/e_2 are computed from their temperature and salinity (S) functions[45] for t_m (eq 1), with S and *in situ* t (used in eq 2) determined independently, e.g., from a codeployed CTD (conductivity, temperature, depth) probe for field deployments. On the basis of field deployments (Performance Tests and Results and Discussion), the mean

https://doi.org/10.1021/acs.est.1c03517
Environ. Sci. Technol. 2021, 55, 14968−14978

(1σ) $\Delta t = t - t_m$ (eq 2) was −1.1 (0.5) °C (n = 1693). The combination of $pH_{T,m}$ with TA or DIC is the most rigorous way to compute the temperature effect for site-specific environmental conditions,[46] especially for large temperature adjustments. The use of the linear temperature correction[46] for small temperature adjustment here is an expedient approach when lacking such ancillary measurements. The sensor uses 4 mM mCP, purified using flash chromatography.[47] Purified mCP (molecular form) was diluted in ∼0.7 M NaCl with addition of 1 M NaOH to facilitate dissolution and achieve a final, potentiometrically monitored pH ∼ 8 (20 °C). Stored in the dark in glass vials, the dye solution is stable for several years (SI Part A). For deployment, the dye solution was transferred in a dark gastight bag (Flexboy Sartorius AG) connected to the sensor.

2.2. Sensor Hardware. *2.2.1. Microfluidic Platform.* The LOC pH sensor is based on an earlier benchtop/underway system[48] and uses the same microfluidic LOC v3 hardware platform already used in LOC nutrient sensors.[36−38,49] Fluid manipulation and optical measurements take place in a three-layer microfluidic chip constructed from tinted (reducing stray light) poly(methyl methacrylate) (PMMA) and bonded using a solvent method.[50] Fluidic control through 300 × 250 μm (W × H) microfluidic channels is achieved using four solenoid valves (LFNA1250325H, The Lee Company, Connecticut, USA) and a custom-built syringe pump, containing two syringes, mounted directly on the microfluidic chip. A 0.8 m × 300 μm × 250 μm (L × W × H) serpentine mixing channel is milled in the middle layer of the chip, with two thermistors (P60BB203 K Amphenol Advanced Sensors) positioned either side of a 1 cm × 700 μm × 300 μm optical cell (Figure 1). The thermistors were calibrated from 0 to 40 °C in a FLUKE High Precision Bath (Hart Scientific) against an F250 MKII Precision Thermometer (A∑Λ Automatic Systems Laboratories), itself calibrated against a Sea-Bird Scientific temperature probe (SBE 35; accuracy better than ±0.001 °C; www.seabird.com), with a precision (1σ) better than ±0.005 °C.

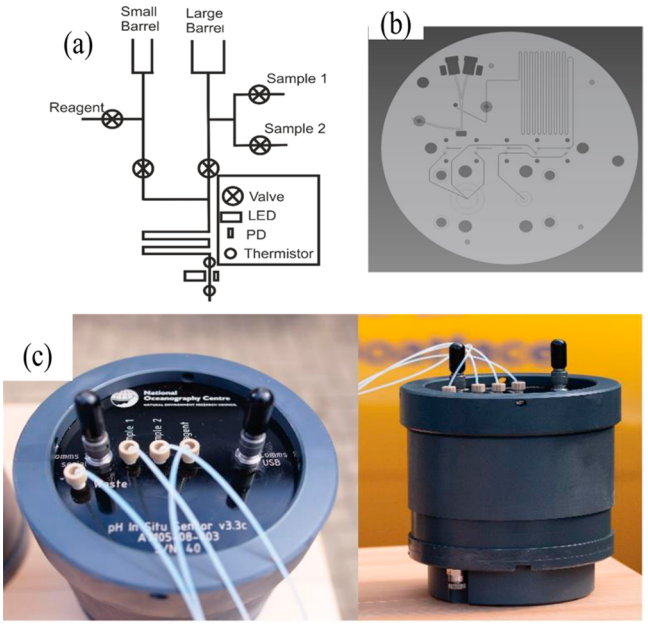

Figure 1. (a) Schematic and (b) CAD design of V3.3c microfluidic LOC; (c) the assembled autonomous pH LOC sensor in its oil-filled casing (125 mm diameter ×195 mm height).

The sensor housing (125 mm diameter by 195 mm height) is filled with mineral oil (Sigma-Aldrich) incorporating an internal pressure-compensating bladder. Its total weight in water is 0.85 kg (3.6 kg in air), and all electronics and mechanical components are pressure tolerant to at least 600 bar. To prevent particles from entering the fluidic channels, the sample is withdrawn through a Millipore Millex syringe filter (33 mm diameter, 0.45 μm pore size) secured on the outside of the sensor housing and replaced after each deployment. There was no evidence to suggest filter clogging during this study or during year-long deployments of LOC nutrient sensors. The sensor is equipped with two sample inlets (Figure 1a) which, if desired, allows the use of an on-board standard (pH buffer) for periodic performance checks. For autonomous deployments, power can be provided by an external battery pack or directly by the observing platform.

2.2.2. Optical setup. Optical measurements are made with two light-emitting diodes (LEDs) (Roithner Lasertechnik GmbH, Vienna) and a photodiode (TSL257, Texas Advanced Optoelectronic Solutions Inc., USA) fixed in position with optical glue (Opti-tec 5012, Intertronics). The LEDs have peak wavelengths at 435 and 590 nm, with peak fwhm (Full Width at Half Maximum) of 15 nm. Measurement discrepancy from the mismatch between the peak wavelengths of the two LEDs and the wavelengths of the mCP absorbance maxima (434 and 578 nm) (SI Part B; Figure S1) is accounted for by calibration (Section 2.3.3). The LEDs are modulated based on time-division multiplexing, (i.e., the two light sources switch on and off alternately in a defined frequency). The signal is demodulated by the detector, allowing light intensity and absorbance quantification at each wavelength.

2.3. Measurement Protocol. *2.3.1. Measurement sequence.* The operation of the sensor is controlled by a Windows-based Graphical User Interface (GUI) written in C. A pH measurement takes place in a four-step, 8 min cycle, with two sample rinses, sample withdrawal (700 μL) and dye injection (3 μL), absorbance measurement, and sample discharge. Slow (57 μL min^{-1}) transfer of the sample-indicator fluid through the serpentine mixer forces the dispersion and diffusion of the indicator into the sample, yielding a Taylor-Aris dispersion curve (Figure 2), which is used to calculate pH and account for the sample pH perturbation caused by the indicator addition.[33,48]

2.3.2. Calculation of absorbance and sample pH correction for indicator perturbation. During each measurement, reference intensity (I^0) is the light intensity measured by the detector (as voltage at 10 Hz) during the first 50 s into the measurement in sample without indicator (Figure 2), which allows compensation for any intrinsic light absorbance of the sample or changes in LED light output. Absorbance is calculated as $A_\lambda = \log\left(\frac{I_\lambda^0}{I_\lambda}\right)$ where λ is wavelength (435 or 590 nm) and I_λ^o and I_λ are, respectively, reference and indicator-sample mixture light intensities at wavelength λ, with measured ratio $R_{meas} = A_{590}/A_{435}$. Absorbance measurements at λ > 700 nm (where mCP has no absorbance) are often used to account for changes in LED light intensity (e.g., drift, noise) or light throughput (e.g., due to sample intrinsic light absorptivity, fouling, etc.).[28,33] However, such issues are accounted for by the I^0 measurement preceding every pH measurement made by the LOC pH sensor (Figure 2). This is

https://doi.org/10.1021/acs.est.1c03517
Environ. Sci. Technol. 2021, 55, 14968−14978

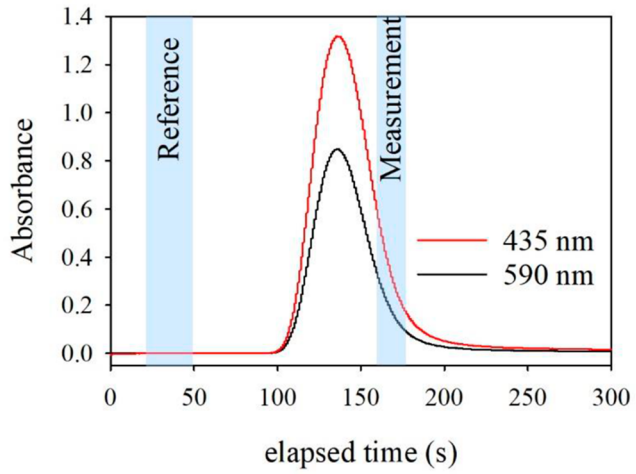

Figure 2. Absorbance vs time during the sample-indicator fluid transit through the optical cell. Shaded areas represent the data segments used for the $pH_{T,m}$ calculation (eq 1).

supported by the pH measurement reproducibility demonstrated by the LOC sensor (Results and Discussion).

Correction for the perturbation of sample pH by the added mCP[33,48] yields the indicator-free R_{meas} of the sample. This is determined from the first derivative of the quadratic fit $A_{590} = a\,(A_{435})^2 + b\,A_{435}$ (Figure S2b) at $A_{435} = 0$ as $R_{meas} = \left(\frac{dA_{590}}{dA_{435}}\right)_{A_{435}=0} = b$ for negligible perturbation as $A_{435} \rightarrow 0$ in the linear part of the absorbance response of the sensor LEDs for $A_{435} > 0.1$ and $A_{590} < 0.6$ in the tail-end of the peak generated during the transit of the diffusive indicator-sample plug through the optical cell (between 150 and 200 s; Figure 2). Compared with alternative methods of accounting for indicator perturbation in laboratory and autonomous pH systems,[28,33,48] this method offers increased precision in the determination of R_{meas} by minimizing noise from regular fluctuations in the light output of the LEDs (Figure S2; Table S2) and yielded comparative results within an average (1σ) difference of −0.00009 (0.00101) pH units, equivalent to −0.0003 (0.0024) (n = 37) difference in R_{meas} (details in SI Part C).

2.3.3. Standardization of R_{meas}. Because mCP absorbance at 590 nm is lower than that at the absorbance maximum (A_{578}) (Figure S1), $R_{meas} = A_{590}/A_{435}$ is lower than the $R = A_{578}/A_{434}$, which necessitates standardization for the calculation of pH_T[51] (eq 1). The R_{meas} in each sensor was standardized in the 0−40 °C range using measurements in two synthetic saline (S = 35) Tris-HCl buffers with different Tris/HCl molality ratios (details in SI Part D), with temperature-dependent buffer pH_T range from 7.3 to 8.8 (Figure S3b). The in-house buffer pH was verified on a Cary 60 UV−vis (Agilent Technologies) spectrophotometer at constant temperature (20 °C) (details in SI Part A). Standardization was achieved via linear regression (Figure S3) of R_{meas} determined in buffer against the R derived by solving eq 1 using the Tris-HCl buffer pH_T[52−54] and the−$\log(K_2e_2)$, e_1, and e_3/e_2 of purified mCP from their respective salinity and temperature functions.[45] The standard error (SE) in R from the regression was better than 0.017. Sample pH_T is computed from (indicator-free, standardized) sample R and eq 1.

2.3.4. Uncertainty of sensor pH measurement. The uncertainty in the sensor-measured pH was computed as combined standard uncertainty[30,55,56] to propagate the standard uncertainties of individual parameters in eqs 1 and 2 (details in SI Part E). The combined standard uncertainty in $pH_{T,m}$ (eq 1) ($u_{pHT,m}$) was thus estimated to be ≤0.006 pH units at pH 8.5, ≤0.007 pH units at pH 8.0, and ≤0.013 pH units at pH 7.5 (Table S4). The three largest contributors to the combined standard uncertainty of $pH_{T,m}$ by >0.001 pH units were the uncertainty in the $-\log(K_2e_2)$ of mCP, the measurement temperature in the sensor optical cell, and R (Table S4). At the constant temperature (25 °C) and salinity (35) of the calculations, the pH-dependent contributor to $u_{pHT,m}$ above is R, which decreases with decreasing pH and, being inversely related, results in increasing R sensitivity factor for spectrophotometric pH (eq S5) with decreasing pH. Hence, with increasing uncertainty contribution from R, $u_{pHT,m}$will increase with decreasing pH for a given uncertainty in R ($u(R)$). The combined standard uncertainty in the *in situ* pH_T (eq 2) ($u_{pHT,t}$) for the mean $\Delta t = t - t_m$ from the field deployments (Measurement Principle) was estimated to be ≤0.009 pH units at pH 8.5, ≤0.010 pH units at pH 8.0, and ≤0.014 pH units at pH 7.5 (Table S4). In comparison, the total measurement uncertainty of the benchtop spectrophotometric pH method has been estimated to be <0.010 pH units.[28−30]

2.4. Performance Tests. *2.4.1. Validation of pH_T output of LOC sensor in the laboratory.* The analytical performance of the LOC sensor was validated in the laboratory as an extent of conformity with the pH_T measured in seawater samples on a benchtop Cary 60 UV−vis (Agilent Technologies) spectrophotometer at constant temperature (~20 °C) (details in SI Part A). Laboratory comparison between the LOC sensor and the standard benchtop analytical method avoids potential biases due to mismatch between collected field validation samples and seawater analyzed by the sensor. The mean difference (1σ) in measured pH_T between four LOC sensors and the benchtop spectrophotometer at 20 °C in surface North Atlantic seawater (S = 33.84) and two batches of Southampton Water (S = 29.21 and 32.15) was −0.005 (0.007) (range: +0.008 to −0.019, n = 49) pH units.

2.4.2. Field tests at atmospheric pressure and validation by cosampling. The LOC pH sensor was deployed from November 19 to December 16, 2018 and from July 23 to September 24, 2019, suspended at ~1 m depth from the pontoon at the National Oceanography Centre (NOC). The NOC is located at the head of Southampton Water, a tidal estuarine system influenced by the outflow of fresh water from the Itchen, Test, and Hamble Rivers in the south coast of England, UK, providing a robust test of the ability of the sensor to operate under changing environmental conditions. The sensor was scheduled to make hourly measurements connected to a communications box on the pontoon. For the 2018−2019 deployments, an SBE 37-SM MicroCAT C-T (P) Recorder (Sea-Bird Scientific) provided concurrent temperature and salinity measurements necessary for the calculation of *in situ* pH. For the 2019 deployment, a Deep SeapHOx (SN 721−0101; Sea-Bird Scientific) provided higher-frequency pH measurements, temperature, salinity, and dissolved oxygen (DO) concentrations. The field sensor measurements were validated against pH_T measurements of discrete seawater samples (n = 49) using purified mCP on a Cary 60 UV−vis (Agilent Technologies) (n = 28) or a USB4000 (Ocean

https://doi.org/10.1021/acs.est.1c03517
Environ. Sci. Technol. 2021, 55, 14968−14978

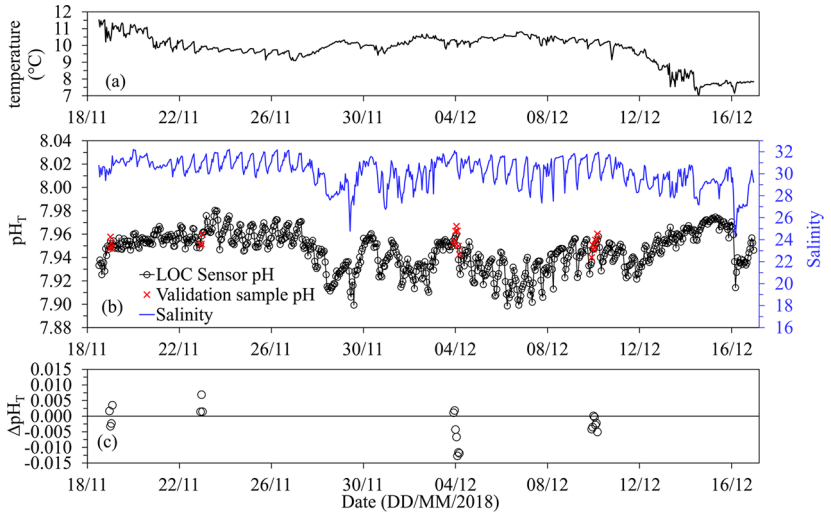

Figure 3. (a) Water temperature, (b) salinity and pH_T from LOC sensor measurements and from measurements in discrete validation seawater samples, and (c) difference in measured pH_T (ΔpH_T) between the LOC sensor and validation seawater samples during field deployments in Southampton Water in November-December 2018. The horizontal solid line in panel (c) indicates $\Delta pH_T = 0$. Note the difference in scale for temperature, salinity, and pH_T with Figure 4.

Optics) spectrophotometer (n = 21). The pH_T of two of the discrete samples was determined on both these benchtop spectrophotometers for comparison (*see* SI Part A). The discrete seawater samples were collected in 40 mL borosilicate glass EPA vials (Cole Palmer) capped with polypropylene screw caps and PTFE/Silicone septa without headspace from a 1.6 L Niskin bottle manually deployed adjacent to the sensor inlets. Sample pH_T was determined in unpreserved seawater samples within 60 min from collection and was converted to pH_T at *in situ* temperature using the linear temperature factor[46] (eq 2).

2.4.3. High pressure tests. Laboratory high pressure test. The performance of the pH sensor at high pressure was assessed in the Systems Reliability Laboratory at NOC in a temperature-controlled (set temperature: 17 °C) pressure vessel controlled by high pressure isostatic equipment (EPSI, Belgium). The sample inlet of the sensor was connected to a synthetic saline (S = 35) nonequimolal (0.06 m Tris, 0.04 m HCl) Tris-HCl buffer solution in a Flexboy (Sartorius AG) bag. The pressure was increased from 1 to 600 bar at 100 bar steps and then decreased to 300 and 100 bar before returning to atmospheric pressure, with a minimum of 17 pH measurements taken at each step. The LOC sensor measurements were processed at the internal temperature of the optical cell (eq 1), including, in this case, the pressure effect on the mCP protonation and absorbance characteristics determined to 827 bar[57] and the pressure dependence of the equimolal Tris-HCl buffer pH_T determined to 200 bar.[58] As a result, the pressure-corrected measured pH_T above 200 bar bears the uncertainty of extrapolation to higher pressures of the equimolal buffer pH_T.

Field high pressure tests. The pH sensor was deployed in Loch Ness, Scotland, UK, in November 2019 integrated on the NOC Autonomous Underwater Vehicle (AUV) Autosub Long Range (ALR) as part of a series of technical integration trials. As Loch Ness is a freshwater environment, the sample inlet of the sensor was connected to a synthetic saline (S = 35) equimolal Tris-HCl buffer. The sensor was controlled and powered by the AUV during a full stepwise descent-ascent from 40 to 200 m water depth (4−19 bar hydrostatic pressure). The ALR conducted lawnmower-pattern surveys at 40, 80, and 200 m depth, holding depth for several hours and allowing for multiple sensor measurements. The LOC sensor pH measurements were processed as outlined for the laboratory high pressure test above.

The pH sensor was deployed attached on a CTD rosette for a series of shallow (~100 and 200 m depth) and deep (~4820 m depth) pH profiles at the Porcupine Abyssal Plain Sustained Observatory (PAP-SO, 49N 16.5W) in the northwest Atlantic Ocean during cruise DY103 on RSS *Discovery* in June−July 2019 (Figure S4). The sensor was powered by a 6000 m depth-rated titanium battery housing containing 4 D-Cell lithium batteries (SAFT LSH-20) and a pressure-triggered switch that allowed power to the sensor when submerged. The sensor measured continuously during each CTD cast. Relevant *S-t-P* and DO data were obtained from a codeployed Sea-Bird Scientific 19 plus CTD probe with an auxiliary SBE-43 DO sensor. The pH_T measurements were corrected to *in situ* temperature and pressure as described above. The *in situ* pH_T data from the sensor were compared with two sets derived from historical data from the past decade (June 2010 and August 2013) available from the world ocean database GLODAPv2[59] for stations near the PAP-SO site between 47−49N and 20W (Figure S4). The historical *in situ* pH_T data were computed from laboratory measurements of pairs of carbonate system parameters (TA and DIC, TA and pH at 25 °C and 1 atm) and dissolved inorganic nutrient concentrations, including CTD *S-t-P* values. The historical *in situ* pH_T values were computed using CO2SYS[60] with the dissociation constants of carbonic acid,[61] bisulfate ion,[62] and hydrogen fluoride,[63] and the total boron concentration[64] in seawater. The combined standard uncertainty of these calculations has been estimated to be ~0.012 pH units.[30]

3. RESULTS AND DISCUSSION

The spectrophotometric determination of seawater pH_T using purified mCP is currently the only analytical method offering precision <0.001 pH units and is generally regarded as the standard operating procedure for ocean pH measurements.[31] The bias in the measurement from uncertainties in the molar

https://doi.org/10.1021/acs.est.1c03517
Environ. Sci. Technol. 2021, 55, 14968−14978

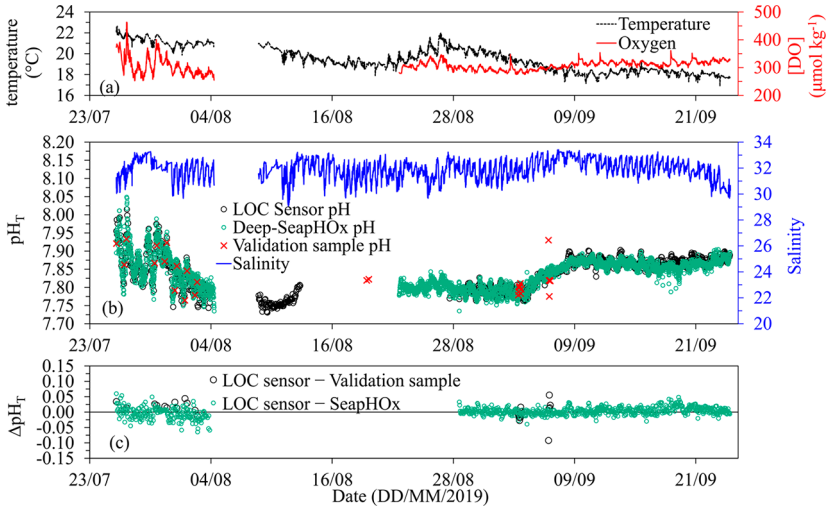

Figure 4. (a) Water temperature and dissolved oxygen, (b) salinity, pH_T from LOC sensor, Deep-SeapHOx, and discrete validation seawater samples, and (c) difference in measured pH_T (ΔpH_T) between the LOC sensor and validation seawater samples, as well as between the LOC sensor and the Deep-SeapHOx during field deployment in Southampton Water in August−September 2019. The horizontal solid line in panel (c) indicates $\Delta pH_T = 0$. The gap in the data represents a break in the deployment due to failure of the LOC power cable. Note the difference in scale for temperature, salinity, pH_T, and ΔpH_T with Figure 3.

absorptivity constants and pK_2 of mCP is currently estimated to be <0.010 pH units[28−30] comparable to the LOC sensor measurement uncertainty (section 2.3.4). As the optical and chemical properties of purified mCP are revised through new empirical determinations, however, historical spectrophotometric pH data can be revised and the bias in measurement quality can be further improved. When used in autonomous systems, spectrophotometric pH measurements are less susceptible to long-term drift, related to changes in light source intensity or indicator delivery, because pH is calculated from the ratio of absorbances at two wavelengths rather than at one wavelength as in classic colorimetry. This is a major advantage for long-term unattended deployments where sensor measurement performance cannot be periodically checked and corrected. The automation of the spectrophotometric method has already been demonstrated with considerable success[32,33] but LOC technology offers the potential for smaller, more autonomous (less power and reagent requirement) and more capable (full ocean depth) sensors without compromising on analytical performance.

Field Deployments in Surface Seawater. During the month-long deployment in early winter 2018 (November 19−December 17), a total of 683 LOC sensor measurements and 21 discrete validation seawater samples were taken. During the deployment, the temperature varied from 7.1 to 11.5 °C (Figure 3a), the salinity varied from 24.2 to 32.2, and the (LOC sensor-determined) *in situ* pH_T ranged from 7.899 to 7.980 (Figure 3b). The short-term (6−8 h; tidal-scale) variability of salinity was within 4 units; that of temperature was within 0.5 °C, while that of *in situ* sensor pH_T was within 0.05 pH units. The mean (1σ) difference between LOC sensor and discrete validation seawater sample pH_T was −0.003 (0.005) pH units (range: − 0.013 to +0.007, $n = 21$) in winter 2018 (Figure 3c).

During the two-month long deployment in late summer 2019 (July 25−September 24), a total of 1010 LOC sensor measurements and 4074 SeapHOx measurements were made and 28 discrete validation seawater samples were taken. During the deployment, the temperature varied from 16.9 to 22.6 °C (Figure 4a) and the salinity from 29.1 to 33.4, while the LOC sensor and SeapHOx *in situ* pH_T ranged from 7.731 to 8.015 and from 7.735 to 8.049, respectively (Figure 4b). The short-term, tidal-scale variability was within 4 units for salinity, similar to the winter deployment, and ∼1.5 °C for temperature, a factor of 3 higher than in winter. pH short-term tidal-scale variability, as recorded by the two sensors, was within 0.10 to 0.20 pH units early in the deployment and within 0.06 pH units toward the end. A gradual decline in water temperature was observed over a monthly time scale, from 11.5 °C to 7−8 °C during the winter 2018 deployment and from 23 to 17.5 °C during the summer 2019 deployment, consistent with the seasonal transition toward colder months (Figures 3a, 4a). No longer-term trend in salinity was evident other than tidal-scale variability. The mean (1σ) difference between LOC sensor and discrete validation seawater sample pH_T was +0.007 (0.028) pH units (range: − 0.092 to +0.055, $n = 26$) in summer 2019 (Figure 4c), which was larger than in winter 2018. The combined mean (1σ) difference for both winter 2018 and summer 2019 was +0.003 (0.022) ($n = 47$). These are comparable with the validation offsets determined in the laboratory (Section 2.4.1)

The mean (1σ) difference between time-matched LOC sensor and Deep-SeapHOx pH_T measurements was +0.002 (0.014) pH units (range: − 0.065 to +0.060, $n = 914$) (Figure 4c), while that between Deep-SeapHOx and validation sample pH_T was +0.007 (0.028) pH units (range: − 0.097 to +0.054, $n = 26$), the same as that between the LOC sensor and validation sample measurements outlined earlier. This indicates short-term (up to 2 months) consistency between the two pH-sensing technologies in the dynamic estuarine-type conditions at the deployment site. The average measurement difference between the Deep-SeapHOx and the validation samples was similar to that of the Deep-Sea DuraFET during the first six months of the SOCCOM program in the Southern Ocean (0.005 ± 0.007 pH units)[21] and in line with the Alliance of Coastal Technologies seawater field evaluations[65] (−0.008 ± 0.029, $n = 84$; − 0.014 ± 0.009, $n = 101$; − 0.001 ± 0.007, $n = 107$). The Deep-SeapHOx used in this study was equipped

https://doi.org/10.1021/acs.est.1c03517
Environ. Sci. Technol. 2021, 55, 14968−14978

only with an external solid state reference electrode[18] which requires reliable real-time salinity measurements for optimum analytical performance.[19,22] Large tidal salinity fluctuations had no apparent effect on the pH measurement quality of the Deep-SeapHOx in this study, highlighting the benefit of the coupling of the SeaFET with the integrated SBE-37 MicroCAT CTD-DO of the SeapHOx package. Comparison of coincident *S-t* measurements made by the Deep-SeapHOx package and the SBE 37-SM MicroCAT C-T (P) (Sea-Bird Scientific) deployed independently on the boat pontoon yielded mean (1σ) differences of −0.08 (0.24) units for salinity (range: −2.13 to +0.95, n = 3143) and −0.03 (0.12)°C for temperature (range: − 0.96 °C to +0.85 °C, n = 3145), suggesting good *S-t* agreement between the two instruments. On fixed observatories such as moorings and seabed landers the LOC pH sensor can provide long-term, high-resolution observations from surface to 6000 m water depth. Because of the small reagent requirement (3 μL per measurement), the sensor's endurance is ultimately limited by the availability of external power.

Laboratory Experiment at Pressure. A total of 261 sensor measurements were made on the Tris-HCl buffer (pH_T = 7.885 at 1 atm (0 bar gauge pressure) and 21.99 (0.62) °C mean (1σ) optical cell temperature). The performance of the sensor was assessed by examining the offset ($\Delta pH_{T,\ Tris}$) between the measured pH_T and the pH_T of the buffer, both pressure-corrected (see High pressure tests) (Figure 5a). At the initial gauge pressure (0.9 bar), mean (1σ) $\Delta pH_{T,\ Tris}$ = +0.0095 (0.0003) pH units (n = 18). During pressurization to 300 bar, $\Delta pH_{T,\ Tris}$ increased to, and remained near-constant thereafter to 600 bar at, + 0.0147 (0.0007) pH units (n = 72). During depressurization to 300 and 100 bar, $\Delta pH_{T,\ Tris}$ increased further to +0.0171 (0.0007) (n = 35) pH units and decreased to +0.0116 (0.0003) (n = 96) pH units upon final depressurization to 0.9 bar. The offset under pressure varied within 0.010 pH units during the pressurization and depressurization cycles. Furthermore, it was higher than the benchtop check measurements on buffers (SI Part A) and the combined standard uncertainty (~0.008 pH units) computed from that of the LOC sensor measurement (~0.006 pH units; Table S4) and the in-house buffer (0.005 pH units; SI Part D), all at 1 atm. Although the behavior of the LOC sensor during the laboratory pressure tests merits further investigation, pH_T measurements were within 0.010−0.020 pH units from the pH_T of the Tris-HCl buffer and showed typically high reproducibility (<0.001 pH units) throughout, demonstrating good sensor performance along pressure gradients to 600 bar.

Field Deployments at Pressure. During the field deployment in Loch Ness in November−December 2019, the LOC pH sensor, integrated on the ALR AUV, measured Tris-HCl buffer pH during a single dive at 40 and 200 m depth (4 and 19 bar hydrostatic pressure), with a pressure-corrected average $\Delta pH_{T,\ Tris}$ = +0.0036 pH units and a reproducibility of 0.0006 pH unit (n = 61) (Figure 5b). The sensor was successfully operated by the AUV, measuring on command and receiving *T*, *S*, and *P* data from the AUV CTD sensor, which, during a science mission at sea, will be used by the LOC pH sensor to calculate *in situ* pH_T. Measurement precision remained good, unaffected by vehicle behavior and interferences such as changing vehicle velocity, depth, or mode of operation.

During the field deployment at PAP-SO, the LOC sensor-measured *in situ* pH_T varied between a maximum of ~8.15

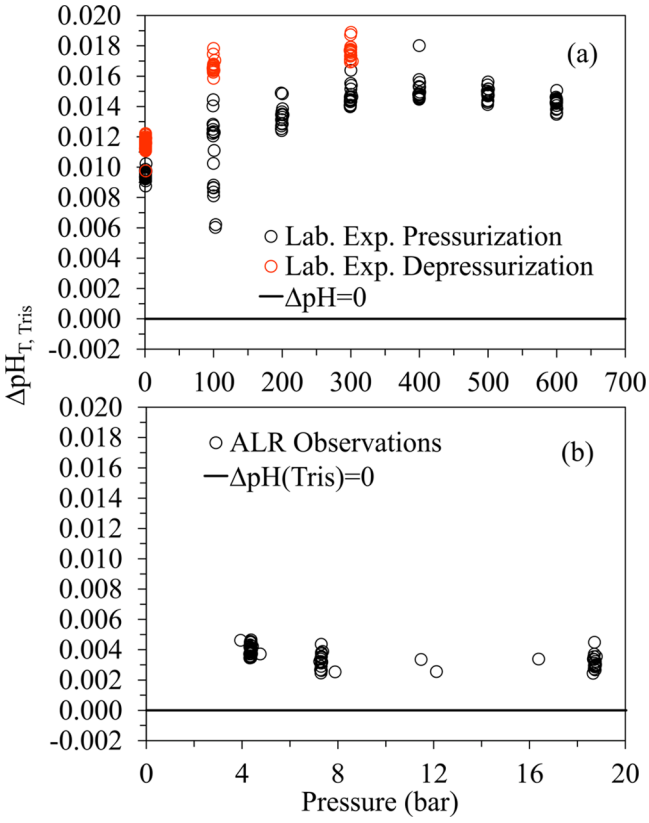

Figure 5. Offset of pressure-corrected LOC sensor-measured pH_T from the pH_T of Tris-HCl buffer as a function of gauge pressure (pressure above atmospheric) (a) during laboratory-controlled pressurization-depressurization experiment and (b) during deployment on an ALR in Loch Ness in November−December 2019 during dives to specific depths for several hours. Note the different scale of the *x*-axis in panels a and b.

near the ocean surface to subsurface and deep water minima of ~7.90 at ~750 m and ~4820 m depth, respectively, with a slight increase to a broad deep maximum of ~7.97 between 1500 and 3000 m depth (Figure 6a). The subsurface minimum occurred within the DO minimum layer in the lower part of the halocline and thermocline (Figure S5). All the available oceanic profiles (pH_T, *S*, *t*, DO) from the PAP-SO site (Figures 6a, S5) exhibited good short-term reproducibility between successive deployments from 25 June to 4 July 2019. The consistency among the LOC sensor pH profiles was within 0.005 pH units except in the upper 1000 m where vertical gradients of physical and chemical parameters were strong (Figures 6, S5). Comparison with the most recent available historical data derived from the GLODAPv2 database from stations near the PAP-SO site (Figure S4) shows good correspondence of the main features of surface and deep subsurface maxima, as well as the deep subsurface and deepest pH_T minima (Figure 6a). The LOC sensor-measured pH_T was generally within 0.020 pH units from the computed historical pH_T values, especially deeper than 1500 m. This discrepancy is comparable in magnitude to the combined standard uncertainty (≤0.016 pH units) of the LOC sensor measurement (≤0.010 pH units at pH ~ 8; Table S4) and related computations on the historical data[30] (~0.012) but tended to exceed it toward the sea-surface (<1500 m depth; Figure 6b). Although the aim of this deployment was to validate the performance of the LOC pH sensor at high pressure, the close

https://doi.org/10.1021/acs.est.1c03517
Environ. Sci. Technol. 2021, 55, 14968−14978

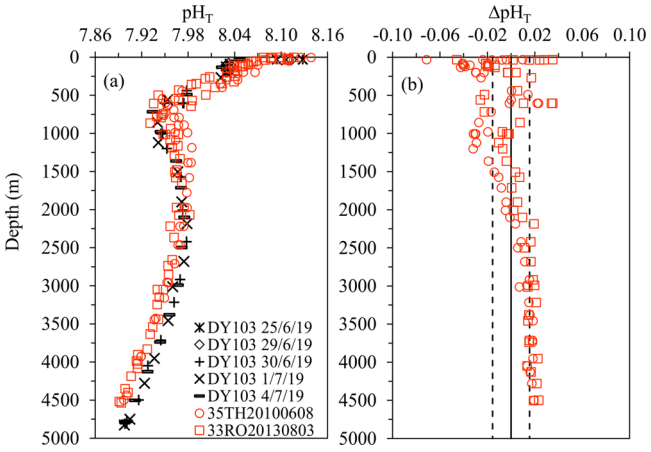

Figure 6. (a) *In situ* water column pH (total proton scale) profiles with depth measured by the LOC sensor during five deployments at the Porcupine Abyssal Plain Sustained Observatory during cruise DY103 on RV *Discovery* in June–July 2019. The *in situ* pH profiles from the past decade in nearby hydrographic stations (Figure S4) were computed as outlined in the main text (cruise expocode 33RO20130803, stations visited on August 11 and 12, 2013, four observations with flag 4 (bad) TA measurements were excluded; cruise expocode 35TH20100608, stations visited on June 18, 2010). (b) Difference (ΔpH_T) in *in situ* pH (total proton scale) between LOC sensor measurements and the computed historical values shown in panel a. The vertical solid line indicates $\Delta pH_T = 0$. The vertical dashed lines indicate combined standard uncertainty for the LOC sensor-measured pH and the computed historical values as outlined in main text.

agreement in measured pH between different casts and historical data highlights the potential of this sensor for obtaining high quality *in situ* pH data during ship-based scientific campaigns. *In situ* measurements in the subsurface and deep ocean eliminate measurement biases related to depressurisation of *ex situ* sample collection and *ex situ* pH extrapolation to *in situ* temperature and pressure.

Further Developments. The autonomous LOC pH sensor described here is the first of its kind capable of high quality, *in situ*, spectrophotometric pH measurements integrated on autonomous underwater vehicles and stationary platforms from surface waters to 6000 m depth. The sensor is currently being trialled at sea, integrated on autonomous vehicles such as the Kongsberg Seaglider, the Autosub Long Range, and the Liquid Robotics Waveglider, while work is currently underway for integration on NKE profiling floats. Coupled with 6000 m depth-rated LOC TA or LOC DIC sensors, currently under validation (see CarCASS project, https://projects.noc.ac.uk/oceanids/sensors-grants), this new technology will transform our capability to observe ocean acidification and the oceanic inorganic carbon system at higher spatiotemporal resolution throughout the oceanic water column and at lower cost than traditional ship-based observing. The LOC pH sensor uses a generic hardware platform shared by several other, more complex analytical assays.[37,38,66] The relative simplicity of the spectrophotometric pH technique allows further hardware simplification and miniaturization, saving overall space and power requirements and reducing cost. Future sensor designs include monochromatic filters and LEDs with peak outputs closer to the absorbance maxima of mCP potentially eliminating the need for optical calibrations and reducing measurement uncertainty. Current optimization work is also focused on reducing measurement duration to enable higher spatial resolution on fast moving and profiling platforms such as gliders and floats. The version of LOC pH sensor described in this work is now commercially available from ClearWater Sensors Ltd.

■ ASSOCIATED CONTENT

Supporting Information

The Supporting Information is available free of charge at https://pubs.acs.org/doi/10.1021/acs.est.1c03517.

Benchtop spectrophotometric pH measurements, absorbance spectra of LOC pH sensor LEDs and *meta*-cresol purple, correction for perturbation of sample pH from indicator addition on LOC sensor, buffer preparation and sensor calibration, computation of the uncertainty in the pH_T determination by the LOC pH sensor, field data (PDF)

■ AUTHOR INFORMATION

Corresponding Author

Socratis Loucaides − *National Oceanography Centre, European Way, SO14 3ZH Southampton, U.K.;* orcid.org/0000-0001-5285-660X; Phone: +44 (0)23 8059 6551; Email: s.loucaides@noc.ac.uk

Authors

Tianya Yin − *National Oceanography Centre, European Way, SO14 3ZH Southampton, U.K.; University of Southampton, Waterfront Campus, European Way, SO14 3ZH Southampton, U.K.;* Present Address: Peking University, 5 Yiheyuan Road, Haidian District, Beijing, China

Stathys Papadimitriou − *National Oceanography Centre, European Way, SO14 3ZH Southampton, U.K.*

Victoire M.C. Rérolle − *National Oceanography Centre, European Way, SO14 3ZH Southampton, U.K.;* Present Address: Fluidion SAS, 94 Av. Du General de Gaulle 9400 Creteil

Martin Arundell − *National Oceanography Centre, European Way, SO14 3ZH Southampton, U.K.*

Christopher L. Cardwell − *National Oceanography Centre, European Way, SO14 3ZH Southampton, U.K.*

John Walk − *National Oceanography Centre, European Way, SO14 3ZH Southampton, U.K.*

Martin R. Palmer − *University of Southampton, Waterfront Campus, European Way, SO14 3ZH Southampton, U.K.*

Sara E. Fowell − *National Oceanography Centre, European Way, SO14 3ZH Southampton, U.K.*

Allison Schaap − *National Oceanography Centre, European Way, SO14 3ZH Southampton, U.K.*

Matthew C. Mowlem − *National Oceanography Centre, European Way, SO14 3ZH Southampton, U.K.*

Complete contact information is available at: https://pubs.acs.org/10.1021/acs.est.1c03517

Author Contributions

T.Y., V.R., M.A., C.L.C., J.W., S.E.F, A.S., M.C.M., and S.L. contributed to the development of the LOC pH sensor. S.P., S.L., C.L.C. and M.A. contributed to the laboratory and field experiments and S.P. performed the data and uncertainty analysis reported in this work. S.L., S.P., and T.Y. composed this manuscript and all authors contributed to its revision.

https://doi.org/10.1021/acs.est.1c03517
Environ. Sci. Technol. 2021, 55, 14968−14978

Funding

This work has received funding from the European Union Horizon 2020 research and innovation program under grant agreements No. 654462 (STEMM-CCS) and No. 633211 (AtlantOS), the European Union Seventh Framework Programme (FP7/2007−2013) under Grant Agreement No. 61414 (SenseOcean), and the National Environment Research Council UK, Grant Reference NE/P02081X/1 (CarCASS) and NE/R015953/1 (CLASS). The PhD studentship of Tianya Yin was funded by the China Scholarship Council (certificate no. 201306320178).

Notes

The authors declare the following competing financial interest(s): Matt Mowlem is a director, CTO, shareholder and employee of ClearWater Sensors Ltd. that manufacture and sell Lab on Chip chemical sensors (including pH) utilising intellectual property licensed from the University of Southampton and the National Oceanography Centre. This IP is used in the sensors described in this paper. Matt maintains employment in the NOC with interactions governed by a detailed conflict of interest policy. Chris Cardwell is a shareholder and employee of ClearWater Sensors Ltd. and also maintains employment in the NOC with interactions governed by the same conflict of interest policy.

■ ACKNOWLEDGMENTS

The authors would like to thank the engineering team of the Ocean Technology and Engineering Group at the NOC (Kevin Saw, Robin Brown, Jim Wyatt, Urška Martinčič, and Stephen Shorter) for technical input throughout the development and testing of the LOC pH sensor and Euan Wilson for assisting with collection and analysis of validation samples. We would also like to thank the crew of RV *Discovery* for integrating and testing the LOC pH sensor on the ship's CTD rosette and Jake Ludgate and the engineers of the Marine Autonomous Robotic Systems (MARS) group at NOC for the integration and testing of the sensor on the ALR. Lastly, we would like to express our gratitude for the detailed and constructive reviews provided by the reviewers, which have undoubtedly improved the quality of this work.

■ REFERENCES

(1) Gattuso, J.-P.; Hansson, L. *Ocean Acidification.* 326p, Oxford University Press Inc.: 2011.

(2) Gruber, N.; Clement, D.; Carter, B. R.; Feely, R. A.; van Heuven, S.; Hoppema, M.; Ishii, M.; Key, R. M.; Kozyr, A.; Lauvset, S. K.; Lo Monaco, C.; Mathis, J. T.; Murata, A.; Olsen, A.; Perez, F. F.; Sabine, C. L.; Tanhua, T.; Wanninkhof, R. The oceanic sink for anthropogenic CO_2 from 1994 to 2007. *Science* **2019**, *363*, 1193−1199.

(3) Caldeira, K.; Wickett, M. E. Ocean model predictions of chemistry changes from carbon dioxide emissions to the atmosphere and ocean. *J. Geophys. Res.* **2005**, *110*, 2671 DOI: 10.1029/2004JC002671.

(4) Doney, S. C.; Fabry, V. J.; Feely, R. A.; Kleypas, J. A. Ocean Acidification: The Other CO2 Problem. *Annu. Rev. Mar. Sci.* **2009**, *1*, 169−192.

(5) Fabry, V. J. OCEAN SCIENCE: Marine Calcifiers in a High-CO2 Ocean. *Science* **2008**, *320*, 1020−1022.

(6) Fabry, V. J.; McClintock, J. B.; Mathis, J. T.; Grebmeier, J. M. Ocean Acidification at High Latitudes: The Bellweather. *Oceanography* **2009**, *22*, 160−171.

(7) Fabry, V. J.; Seibel, B. A.; Feely, R. A.; Orr, J. C. Impacts of ocean acidification on marine fauna and ecosystem processes. *ICES J. Mar. Sci.* **2008**, *65*, 414−432.

(8) Guinotte, J. M.; Fabry, V. J. Ocean Acidification and Its Potential Effects on Marine Ecosystems. *Ann. N. Y. Acad. Sci.* **2008**, *1134*, 320−342.

(9) Orr, J. C.; Fabry, V. J.; Aumont, O.; Bopp, L.; Doney, S. C.; Feely, R. A.; Gnanadesikan, A.; Gruber, N.; Ishida, A.; Joos, F.; Key, R. M.; Lindsay, K.; Maier-Reimer, E.; Matear, R.; Monfray, P.; Mouchet, A.; Najjar, R. G.; Plattner, G.-K.; Rodgers, K. B.; Sabine, C. L.; Sarmiento, J. L.; Schlitzer, R.; Slater, R. D.; Totterdell, I. J.; Weirig, M.-F.; Yamanaka, Y.; Yool, A. Anthropogenic ocean acidification over the twenty-first century and its impact on calcifying organisms. *Nature* **2005**, *437*, 681−686.

(10) Hofmann, G. E.; Barry, J. P.; Edmunds, P. J.; Gates, R. D.; Hutchins, D. A.; Klinger, T.; Sewell, M. A. The Effect of Ocean Acidification on Calcifying Organisms in Marine Ecosystems: An Organism-to-Ecosystem Perspective. *Annu. Rev. Ecol. Evol. Syst.* **2010**, *41*, 127−147.

(11) Waldbusser, G. G.; Hales, B.; Langdon, C. J.; Haley, B. A.; Schrader, P.; Brunner, E. L.; Gray, M. W.; Miller, C. A.; Gimenez, I. Saturation-state sensitivity of marine bivalve larvae to ocean acidification. *Nat. Clim. Change* **2015**, *5*, 273.

(12) McLaughlin, K.; Weisberg, S. B.; Dickson, A. G.; Hofmann, G. E.; Newton, J. A.; Aseltine-Neilson, D.; Barton, A.; Cudd, S.; Feely, R. A.; Jefferds, I. W.; Jewett, E. B.; King, T.; Langdon, C. J.; McAfee, S.; Pleschner-Steele, D.; Steele, B. Core Principles of the California Current Acidification Network Linking Chemistry, Physics, and Ecological Effects. *Oceanography* **2015**, *28*, 160−169.

(13) Newton, J. A., Feely, R. A., Jewett, E. B., Williamson, P.; Mathis, J. T. Global Ocean Acidification Network: Requirements and Governance Plan. *57* GOA-ON, **2014**.

(14) Zeebe, R. E. History of Seawater Carbonate Chemistry, Atmospheric CO2, and Ocean Acidification. *Annu. Rev. Earth Planet. Sci.* **2012**, *40*, 141−165.

(15) Bockmon, E. E.; Dickson, A. G. An inter-laboratory comparison assessing the quality of seawater carbon dioxide measurements. *Mar. Chem.* **2015**, *171*, 36−43.

(16) Martz, T. R.; Daly, K. L.; Byrne, R. H.; Stillman, J. H.; Turk, D. Technology for ocean acidification research: Needs and Availability. *Oceanography* **2015**, *28*, 40−47.

(17) Johnson, K. S.; Jannasch, H. W.; Coletti, L. J.; Elrod, V. A.; Martz, T. R.; Takeshita, Y.; Carlson, R. J.; Connery, J. G. Deep-Sea DuraFET: A Pressure Tolerant pH Sensor Designed for Global Sensor Networks. *Anal. Chem.* **2016**, *88*, 3249−3256.

(18) Martz, T. R.; Connery, J. G.; Johnson, K. S. Testing the Honeywell Durafet® for seawater pH applications. *Limnol. Oceanogr.: Methods* **2010**, *8*, 172−184.

(19) Bresnahan, P. J.; Martz, T. R.; Takeshita, Y.; Johnson, K. S.; LaShomb, M. Best practices for autonomous measurement of seawater pH with the Honeywell Durafet. *Methods Oceanogr.* **2014**, *9*, 44−60.

(20) Takeshita, Y.; Martz, T. R.; Johnson, K. S.; Dickson, A. G. Characterization of an Ion Sensitive Field Effect Transistor and Chloride Ion Selective Electrodes for pH Measurements in Seawater. *Anal. Chem.* **2014**, *86*, 11189−11195.

(21) Johnson, K. S.; Plant, J. N.; Coletti, L. J.; Jannasch, H. W.; Sakamoto, C. M.; Riser, S. C.; Swift, D. D.; Williams, N. L.; Boss, E.; Haëntjens, N.; Talley, L. D.; Sarmiento, J. L. Biogeochemical sensor performance in the SOCCOM profiling float array. *J. Geophys. Res.: Oceans* **2017**, *122*, 6416−6436.

(22) Rérolle, V.; Ruiz-Pino, D.; Rafizadeh, M.; Loucaides, S.; Papadimitriou, S.; Mowlem, M.; Chen, J. Measuring pH in the Arctic Ocean: Colorimetric method or SeaFET? *Methods Oceanogr.* **2016**, *17*, 32−49.

(23) Gonski, S. F.; Cai, W.-J.; Ullman, W. J.; Joesoef, A.; Main, C. R.; Pettay, D. T.; Martz, T. R. Assessment of the suitability of Durafet-based sensors for pH measurement in dynamic estuarine environments. *Estuarine, Coastal Shelf Sci.* **2018**, *200*, 152−168.

(24) Juranek, L. W.; Feely, R. A.; Gilbert, D.; Freeland, H.; Miller, L. A. Real-time estimation of pH and aragonite saturation state from Argo profiling floats: Prospects for an autonomous carbon observing strategy. *Geophys. Res. Lett.* **2011**, *38*, L17603.
(25) Takeshita, Y.; Johnson, K. S.; Martz, T. R.; Plant, J. N.; Sarmiento, J. L. Assessment of Autonomous pH Measurements for Determining Surface Seawater Partial Pressure of CO2. *J. Geophys. Res.: Oceans* **2018**, *123*, 4003−4013.
(26) Clayton, T. D.; Byrne, R. H. Spectrophotometric seawater pH measurements: total hydrogen ion concentration scale calibration of m-cresol purple and at-sea results. *Deep Sea Res., Part I* **1993**, *40*, 2115−2129.
(27) Robert-Baldo, G. L.; Morris, M. J.; Byrne, R. H. Spectrophotometric determination of seawater pH using phenol red. *Anal. Chem.* **1985**, *57*, 2564−2567.
(28) Carter, B. R.; Radich, J. A.; Doyle, H. L.; Dickson, A. G. An automated system for spectrophotometric seawater pH measurements. *Limnol. Oceanogr.: Methods* **2013**, *11*, 16−27.
(29) Marion, G. M.; Millero, F. J.; Camoes, M. F.; Spitzer, P.; Feistel, R.; Chen, C. T. A. pH of seawater. *Mar. Chem.* **2011**, *126*, 89−96.
(30) Orr, J. C.; Epitalon, J.-M.; Dickson, A. G.; Gattuso, J.-P. Routine uncertainty propagation for the marine carbon dioxide system. *Mar. Chem.* **2018**, *207*, 84−107.
(31) Dickson, A. G., Sabine, C. L.; Christian, J. R. *Guide to Best Practices for Ocean CO_2 Measurements. Vol. 3* 191p, PICES Special Publication: 2007.
(32) Martz, T. R.; Carr, J. J.; French, C. R.; DeGrandpre, M. D. A submersible autonomous sensor for spectrophotometric pH measurements of natural waters. *Anal. Chem.* **2003**, *75*, 1844−1850.
(33) Seidel, M. P.; DeGrandpre, M. D.; Dickson, A. G. A sensor for in situ indicator-based measurements of seawater pH. *Mar. Chem.* **2008**, *109*, 18−28.
(34) Manz, A.; Graber, N.; Widmer, H. M. Miniaturized total chemical analysis systems: A novel concept for chemical sensing. *Sens. Actuators, B* **1990**, *1*, 244−248.
(35) Nightingale, A. M.; Beaton, A. D.; Mowlem, M. C. Trends in microfluidic systems for in situ chemical analysis of natural waters. *Sens. Actuators, B* **2015**, *221*, 1398−1405.
(36) Beaton, A. D.; Cardwell, C. L.; Thomas, R. S.; Sieben, V. J.; Legiret, F.-E.; Waugh, E. M.; Statham, P. J.; Mowlem, M. C.; Morgan, H. Lab-on-Chip Measurement of Nitrate and Nitrite for In Situ Analysis of Natural Waters. *Environ. Sci. Technol.* **2012**, *46*, 9548−9556.
(37) Clinton-Bailey, G. S.; Grand, M. M.; Beaton, A. D.; Nightingale, A. M.; Owsianka, D. R.; Slavik, G. J.; Connelly, D. P.; Cardwell, C. L.; Mowlem, M. C. A Lab-on-Chip Analyzer for in Situ Measurement of Soluble Reactive Phosphate: Improved Phosphate Blue Assay and Application to Fluvial Monitoring. *Environ. Sci. Technol.* **2017**, *51*, 9989−9995.
(38) Geißler, F.; Achterberg, E. P.; Beaton, A. D.; Hopwood, M. J.; Clarke, J. S.; Mutzberg, A.; Mowlem, M. C.; Connelly, D. P. Evaluation of a Ferrozine Based Autonomous in Situ Lab-on-Chip Analyzer for Dissolved Iron Species in Coastal Waters. *Front. Mar. Sci.* **2017**, *4*, 322 DOI: 10.3389/fmars.2017.00322.
(39) Milani, A.; Statham, P. J.; Mowlem, M. C.; Connelly, D. P. Development and application of a microfluidic in-situ analyzer for dissolved Fe and Mn in natural waters. *Talanta* **2015**, *136*, 15−22.
(40) Beaton, A. D.; Wadham, J. L.; Hawkings, J.; Bagshaw, E. A.; Lamarche-Gagnon, G.; Mowlem, M. C.; Tranter, M. High-Resolution in Situ Measurement of Nitrate in Runoff from the Greenland Ice Sheet. *Environ. Sci. Technol.* **2017**, *51*, 12518−12527.
(41) Vincent, A. G.; Pascal, R. W.; Beaton, A. D.; Walk, J.; Hopkins, J. E.; Woodward, E. M. S.; Mowlem, M.; Lohan, M. C. Nitrate drawdown during a shelf sea spring bloom revealed using a novel microfluidic in situ chemical sensor deployed within an autonomous underwater glider. *Mar. Chem.* **2018**, *205*, 29−36.
(42) Ramirez-Llodra, E.; Brandt, A.; Danovaro, R.; De Mol, B.; Escobar, E.; German, C. R.; Levin, L. A.; Martinez Arbizu, P.; Menot, L.; Buhl-Mortensen, P.; Narayanaswamy, B. E.; Smith, C. R.; Tittensor, D. P.; Tyler, P. A.; Vanreusel, A.; Vecchione, M. Deep, diverse and definitely different: unique attributes of the world's largest ecosystem. *Biogeosciences* **2010**, *7*, 2851−2899.
(43) Levin, L. A.; Bett, B. J.; Gates, A. R.; Heimbach, P.; Howe, B. M.; Janssen, F.; McCurdy, A.; Ruhl, H. A.; Snelgrove, P.; Stocks, K. I.; Bailey, D.; Baumann-Pickering, S.; Beaverson, C.; Benfield, M. C.; Booth, D. J.; Carreiro-Silva, M.; Colaço, A.; Eblé, M. C.; Fowler, A. M.; Gjerde, K. M.; Jones, D. O. B.; Katsumata, K.; Kelley, D.; Le Bris, N.; Leonardi, A. P.; Lejzerowicz, F.; Macreadie, P. I.; McLean, D.; Meitz, F.; Morato, T.; Netburn, A.; Pawlowski, J.; Smith, C. R.; Sun, S.; Uchida, H.; Vardaro, M. F.; Venkatesan, R.; Weller, R. A. Global Observing Needs in the Deep Ocean. *Front. Mar. Sci.* **2019**, *6*, 241 DOI: 10.3389/fmars.2019.00241.
(44) Blackford, J.; Artioli, Y.; Clark, J.; de Mora, L. Monitoring of offshore geological carbon storage integrity: Implications of natural variability in the marine system and the assessment of anomaly detection criteria. *Int. J. Greenhouse Gas Control* **2017**, *64*, 99−112.
(45) Liu, X.; Patsavas, M. C.; Byrne, R. H. Purification and Characterization of meta-Cresol Purple for Spectrophotometric Seawater pH Measurements. *Environ. Sci. Technol.* **2011**, *45*, 4862−4868.
(46) Millero, F. J. Thermodynamics of the carbon dioxide system in the oceans. *Geochim. Cosmochim. Acta* **1995**, *59*, 661−677.
(47) Patsavas, M. C.; Byrne, R. H.; Liu, X. W. Purification of meta-cresol purple and cresol red by flash chromatography: Procedures for ensuring accurate spectrophotometric seawater pH measurements. *Mar. Chem.* **2013**, *150*, 19−24.
(48) Rérolle, V. M. C.; Floquet, C. F. A.; Harris, A. J. K.; Mowlem, M. C.; Bellerby, R. R. G. J.; Achterberg, E. P. Development of a colorimetric microfluidic pH sensor for autonomous seawater measurements. *Anal. Chim. Acta* **2013**, *786*, 124−131.
(49) Grand, M. M., Clinton-Bailey, G. S., Beaton, A. D., Schaap, A. M., Johengen, T. H., Tamburri, M. N., Connelly, D. P., Mowlem, M. C.; Achterberg, E. P. A Lab-On-Chip Phosphate Analyzer for Long-term In Situ Monitoring at Fixed Observatories: Optimization and Performance Evaluation in Estuarine and Oligotrophic Coastal Waters. *Front. Mar. Sci. 4*, doi: DOI: 10.3389/fmars.2017.00255 (**2017**).
(50) Ogilvie, I. R. G., Sieben, V. J., Floquet, C. F. A., Mowlem, M. C.; Morgan, H. Rapid prototyping of PMMA microfluidic devices with optically clear solvent polished fluidic channel walls. *EU patent* (**2009**).
(51) Yang, B.; Patsavas, M. C.; Byrne, R. H.; Ma, J. Seawater pH measurements in the field: A DIY photometer with 0.01 unit pH accuracy. *Mar. Chem.* **2014**, *160*, 75−81.
(52) DelValls, T. A.; Dickson, A. G. The pH of buffers based on 2-amino-2-hydroxymethyl-1,3-propanediol ('tris') in synthetic sea water. *Deep Sea Res., Part I* **1998**, *45*, 1541−1554.
(53) Papadimitriou, S.; Loucaides, S.; Rerolle, V. M. C.; Achterberg, E. P.; Dickson, A. G.; Mowlem, M. C.; Kennedy, H. The measurement of pH in saline and hypersaline media at sub-zero temperatures: Characterization of Tris buffers. *Mar. Chem.* **2016**, *184*, 11−20.
(54) Pratt, K. W. Measurement of pHT values of Tris buffers in artificial seawater at varying mole ratios of Tris:Tris·HCl. *Mar. Chem.* **2014**, *162*, 89−95.
(55) ISO/IEC. *Uncertainty of measurement Part 3: Guide to the expression of uncertainty in measurement (GUM:1995)* . (2008).
(56) Ellison, S. L. R.; Williams, A. *Eurachem CITAC guide: Quantifying Uncertainty in Analytical Measurement.*, 3rd ed., 133p, Eurachem: 2012.
(57) Soli, A. L.; Pav, B. J.; Byrne, R. H. The effect of pressure on meta-Cresol Purple protonation and absorbance characteristics for spectrophotometric pH measurements in seawater. *Mar. Chem.* **2013**, *157*, 162−169.
(58) Takeshita, Y.; Martz, T. R.; Coletti, L. J.; Dickson, A. G.; Jannasch, H. W.; Johnson, K. S. The effects of pressure on pH of Tris buffer in synthetic seawater. *Mar. Chem.* **2017**, *188*, 1−5.

(59) Olsen, A.; Key, R. M.; van Heuven, S.; Lauvset, S. K.; Velo, A.; Lin, X.; Schirnick, C.; Kozyr, A.; Tanhua, T.; Hoppema, M.; Jutterström, S.; Steinfeldt, R.; Jeansson, E.; Ishii, M.; Pérez, F. F.; Suzuki, T. The Global Ocean Data Analysis Project version 2 (GLODAPv2) − an internally consistent data product for the world ocean. *Earth Syst. Sci. Data* **2016**, *8*, 297−323.
(60) Lewis, E.; Wallace, D. W. R. *Program Developed for CO_2 System Calculations. 21p (Carbon Dioxide Information Analysis Center*; Oak Ridge National Laboratory, U.S. Department of Energy, U.S.A., 1998.
(61) Lueker, T. J.; Dickson, A. G.; Keeling, C. D. Ocean pCO2 calculated from dissolved inorganic carbon, alkalinity, and equations for K1 and K2: validation based on laboratory measurements of CO2 in gas and seawater at equilibrium. *Mar. Chem.* **2000**, *70*, 105−119.
(62) Dickson, A. G. Standard potential of the reaction: AgCl(s) + 12H2(g) = Ag(s) + HCl(aq), and and the standard acidity constant of the ion HSO4− in synthetic sea water from 273.15 to 318.15 K. *J. Chem. Thermodyn.* **1990**, *22*, 113−127.
(63) Dickson, A. G.; Riley, J. P. The estimation of acid dissociation constants in seawater media from potentionmetric titrations with strong base. I. The ionic product of water — Kw. *Mar. Chem.* **1979**, *7*, 89−99.
(64) Uppström, L. R. The boron/chlorinity ratio of deep-sea water from the Pacific Ocean. *Deep-Sea Res. Oceanogr. Abstr.* **1974**, *21*, 161−162.
(65) ACT. *Performance Verification Statement for the Satlantic SeaFET pH Sensor.* (Alliance for Coastal Technologies, Maryland, USA, 2015).
(66) Beaton, A. D.; Sieben, V. J.; Floquet, C. F. A.; Waugh, E. M.; Bey, S. A. K.; Ogilvie, I. R. G.; Mowlem, M. C.; Morgan, H. An automated microfluidic colourimetric sensor applied in situ to determine nitrite concentration. *Sens. Actuators, B* **2011**, *156*, 1009−1014.

https://doi.org/10.1021/acs.est.1c03517
Environ. Sci. Technol. 2021, 55, 14968−14978